Experimental and modelling studies for the validation of the mechanistic basis of the Local Effect Model

F. TOMMASINO([1])([2])([3])(*)

([1]) *Department of Physics, University of Trento - Trento, Italy*
([2]) *INFN, Trento Institute For Fundamental Physics and Applications (TIFPA)*
    Trento, Italy
([3]) *Biophysics Department, GSI Helmholtzzentrum für Schwerionenforschung*
    Darmstadt, Germany

Summary. — This review will summarize results obtained in the recent years applying the Local Effect Model (LEM) approach to the study of basic radiobiological aspects, as for instance DNA damage induction and repair, and charged particle track structure. The promising results obtained using different experimental techniques and looking at different biological end points, support the relevance of the LEM approach for the description of radiation effects induced by both low- and high-LET radiation. Furthermore, they suggest that nowadays the appropriate combination of experimental and modelling tools can lead to advances in the understanding of several open issues in the field of radiation biology.

1. – Introduction

Modelling biological effects induced by radiation represents historically an important topic of research in radiation biophysics. Being able to describe and to predict the outcomes of a given radiation exposure at different levels of complexity (from the subcellular to the tissue scale) has practical implications ranging from radiation protection, on earth and in open space, to radiation therapy. This implies considering a broad spectrum of radiation types spanning from photons (X- and γ-rays) to neutrons and charged particles, and gets particularly relevant in the context of modern radiotherapy, due to the rapidly growing number of clinical centres where protons, and in few cases carbon ions, are used to irradiate solid tumours [1].

(*) E-mail: `francesco.tommasino@tifpa.infn.it`

Charged-particle therapy (CPT) shows its main advantages in the treatment of deep-seated solid tumours [2]. In fact, the depth-dose profile of charged particles is characterized by the presence of a so-called *entrance channel* where a low amount of dose is released, followed by a narrow region, defined as the *Bragg peak*, where the majority of the dose is deposited. The pronounced increase in Linear Energy Transfer (LET, expressed in keV/μm) toward the end of the range allows coupling the physical selectivity of charged particles with an enhanced biological effectiveness corresponding to the tumour region compared to conventional photon radiation [3]. The Relative Biological Effectiveness (RBE, ratio of photon to charged-particle dose producing the same biological effect) is the parameter adopted in radiation biophysics to quantify this increase in effectiveness. Even though track structure also plays a role when different ions are compared, as a general approximation we can state that RBE increases for increasing LET.

Radiation-induced biological effects are differentially modulated depending on physical and biological parameters. In CPT this is of primary importance when the aim is the calculation of optimized heavy-ion treatment plans and is reflected by the RBE depending on a spectrum of parameters. For this reason, an accurate prediction of RBE values must be performed and integrated in the Treatment Planning System (TPS) allowing the evaluation of biological dose distributions (or RBE-weighed dose, *i.e.* absorbed dose × RBE, expressed as Gy-RBE) to be delivered to patients.

Extensive work on radiobiological modelling has been conducted in the last decades at GSI (Darmstadt) where, from 1997 to 2008 a pilot project was conducted and about 450 patients were irradiated with accelerated carbon ions. The encouraging results obtained during the project motivated the construction of the Heidelberg Ion beam Therapy centre (HIT) where patients are currently treated with protons and carbon ions. In that context, the Local Effect Model (LEM) has been developed by Michael Scholz and co-workers [4], with the aim to predict RBE as a function of physical (*e.g.* particle species, energy, dose) as well as biological (*e.g.* cell or tissue type, end point) parameters. The first version of the LEM is currently adopted in clinical TPS, while several developments have been proposed over the years, up to the most recent version of the model where a mechanistic picture of DNA damage is proposed for the description of biological effects (LEM IV [5]).

In this review a short overview of the LEM basics will be first presented, focusing on the latest version. Recent applications of the model to the analysis of different biological end points will be then summarized and described. A recent study dedicated to the investigation of charged-particle track structure will be presented, where for the first time based on a biological end point (*i.e.* the induction of DNA Double-Strand Breaks in mouse retina tissues) it was possible to measure the track structure of high-energy ions up to about $20\,\mu$m distance from the particle core [6]. Special attention will be then dedicated to the description of DNA damage induction and repair processes, according to the promising results obtained when applying the LEM approach for the analysis of experimental data obtained with different techniques and involving a large spectrum of radiation qualities [7-10].

2. – Basics of the LEM

The basic concept behind the LEM is that the effects of ion irradiation can be predicted by combining the information contained in the photon dose response curve with the information about the microscopic local dose deposition in the target (*i.e.* the cell nucleus) [4]. The microscopic local dose deposition is considered according to an amorphous track structure model. This means that the radial dose profile for a given ion is calculated

by taking into account the local average dose depositions, without directly considering the effect of each single secondary electron produced by the particle in the interaction with target material. Details about track structure in the LEM are reported elsewhere [11]; here it is worth underlining that the release of dose associated to a charged-particle track can be considered to be inversely proportional to the squared distance from the track centre [12]. The information about the local dose in subnuclear compartments is then the starting point to perform cell survival calculations. This leads to the fundamental assumption of the model that equal local doses produce equal biological effects, independent of the primary radiation quality. Starting with the first version (LEM I [4]), where the expected survival level was calculated by simply averaging over the number of lethal events obtained at a given dose, several improvements have been implemented over the years (LEM II [11], LEM III [13]). Finally in 2010 a new version (LEM IV [5]) of the model was released where an additional level of chromatin organization is considered, thus allowing a more mechanistic description of the induced-damage pattern. Survival probability is now the result of a two-step calculation: first the DSB pattern resulting from a given ion irradiation is evaluated, based on the dose deposition inside the cell nucleus; second, the information in terms of DSB pattern is used to scale the effect induced by the ion to that induced by photons, and survival is finally calculated according to a modified Linear Quadratic approach (see Elsässer *et al.* for details [5]).

The cell nucleus is defined in the LEM as a cylinder having a volume of $500\,\mu\mathrm{m}^3$, with its main axis parallel to the ion beam and a radius of about $5\,\mu\mathrm{m}$. The DNA content of a mammalian cell ($\approx 6 \cdot 10^9$ bp) is considered to be homogeneously distributed in the target. In LEM IV, it is also assumed that the higher-order chromatin structure can be approximated with the organization in chromatin loops, each involving about $2\,\mathrm{Mbp}$ of genome [14, 15]. The nuclear volume is thus divided into cubic domains of fixed size ($\approx 500\,\mu\mathrm{m}$ edge length), each containing approximately $2\,\mathrm{Mbp}$ of DNA. From now on, the terms loop and domain will be considered equivalent. In line with the concept of the amorphous track structure, the DNA damage is induced in the nuclear subunits according to the local dose deposition.

Two types of lesions are considered in the LEM as mediators of radiation-induced effects, namely Single Strand Breaks (SSB) and Double Strand Breaks (DSB). Induction yields of $30\,\mathrm{DSB/Gy}$ and $1250\,\mathrm{SSB/Gy}$ resulting from experimental measurements are adopted in the LEM simulations [11]. DSB are believed to be the principal mediator of cell killing, although SSB are induced in much larger numbers. The experimental observation that the induction of DSB is not purely linear, but also shows a quadratic component at high doses, is taken into account in the LEM by the use of the so-called *DSB enhancement factor*, abbreviated as η factor [11], allowing a distinction between *intra-track* (prompt DSB produced by a the same secondary electron) and *inter-track* DSB (generated by two independent secondary electrons, each producing a SSB on one of the opposite DNA strands) [16]. The contribution of the η factor to the actual number of induced DSB gets relevant only when the local dose is very high, as in case of high-LET irradiation.

According to the loop/domain structure, two different classes of DSB are defined in the LEM IV, namely *isolated* (iDSB) and *clustered* DSB (cDSB). An iDSB is defined as a single DSB induced in a loop, while a cDSB corresponds to the simultaneous presence of two or more DSB (fig. 1). Intuitively, a cDSB is expected to represent a more severe lesion for the cell to be rejoined compared to an iDSB, since it produces the loss of the integrity of the loop structure, and it could eventually result in the loss of DNA fragments. This picture is essentially shared with the Giant LOop Binary LEsion model (GLOBLE [17]),
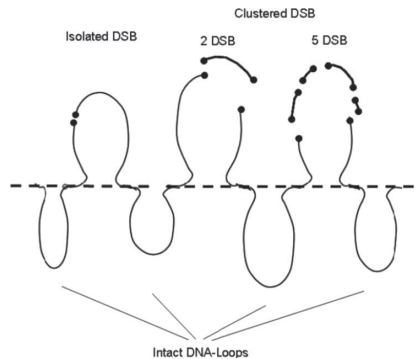
Fig. 1. – Definition of DSB classes in the context of chromatin loop organization: iDSB (left) and cDSB (right) are classified according to whether one or more than one DSB are induced in a loop/domain, respectively. Adapted with permission from Friedrich *et al.* [17].

where nevertheless the additional concept of a different lethality attributed to iDSB and cDSB is used to finally derive survival probability. This approach has been recently shown to be consistent with the linear-quadratic shape of cell survival curves at low LET [18]. Moreover, evidence that clustering of DSB at the micrometre scale could affect the repair kinetics has been reported by Neumaier *et al.* [19], together with the concept of repair centres for the processing of multiple DSB. Based on these considerations, the survival probability after irradiation is calculated in the LEM based on the induced fractions of cDSB (the so-called *cluster index*, details elsewhere [18]).

The loop organization and the local density of DSB at the micrometre scale are clearly identified as key aspects of the model. The results obtained up to now in the comparison of model predictions to measured survival data support the validity of the proposed approach [17, 18, 20]. Based on these assumptions, extensive experimental and modelling work has been carried out in recent years looking for a more direct validation of the mechanistic picture of DNA damage on which the LEM is currently built. The main results will be summarized and discussed in the next sections.

3. – Track structure reconstruction based on γH2AX foci analysis

An accurate description of the track structure associated to charged particles is an aspect of primary importance for radiobiological modelling related to radiation protection and to CPT. Apart from the amorphous track structure approach adopted in the LEM, different strategies are also possible. For instance, MC codes are often used tracking each single secondary electron produced in the interaction of the primary ion with target material [21, 22]. However, experimental data needed for benchmarking of simulated dose profiles in materials of biological relevance are largely missing. This is because gas-filled detectors are usually adopted to measure charged-particle tracks, and results are then scaled to water-like materials taking into account the different densities [12]. However, this is quite a strong approximation.

We recently presented a study where mouse retina tissue was employed to characterize the track structure associated to high energetic heavy ions (*i.e.* titanium ions) [6]. γH2AX foci analysis was adopted to measure DNA damage induction associated to the particle tracks. In fact, the γH2AX assay is currently one of the most diffuse assays for

the study of DSB induction [23, 24]. This is based on the phosphorylation of H2AX histone proteins following DSB induction. An octamer of histone proteins is the basic unit of nucleosomes, sphere-like structures around which chromatin is wrapped. The phosphorylation involves an extended DNA region surrounding the DSB (order of $\approx$Mbp), thus giving rise to the so-called $\gamma H2AX$ foci. With appropriate antibody staining, these foci can be marked with fluorescent probes and then measured with microscopy or flow cytometry techniques [25]. γH2AX foci were used here as a marker to identify the position of DSB. The information in terms of DSB induction at a given distance from the track centre was then converted into a dose value. Experimental data were compared to predictions obtained with the LEM amorphous track structure model. The choice of mouse retina tissue was motivated by these cells being characterized by the nucleus covering most part of the overall cell volume, with a limited amount of surrounding cytoplasm. Thus, they represent an ideal almost-continuous target for the study of DNA damage. At the same time, being LET proportional to the square of the charge and the track radius proportional to the energy, heavy charged particles accelerated at high energies combine a high LET with a large track radius. In the case of titanium ions used in the experiments, the LET was in the range 114–129 keV/μm (1 GeV/u and 0.8 GeV/u, respectively), while the outer track radius was in the order of several millimiters.

Additional aim of the study was the investigation of DNA repair in two distinct track structure regions, namely particle *core* and *penumbra*. The first refers to that region in close proximity to the particle centre where DNA damage is mostly induced by low energy secondary electrons, therefore representing the high LET (densely ionizing) component associated to the ion. On the contrary, particle penumbra extends beyond that inner region and the dose release is due here to the high-energy secondary electrons (also called δ-electrons). These electrons have a residual range of several micrometres, and represent the sparsely ionizing (low LET, photon-like) component of the track structure. Consequently, a different behavior is expected in the two regions in terms of DNA repair, with the DSB induced in the inner volume being more difficult to repair compared to that in the penumbra, and thus persisting for a longer time.

Here we focus on the description of the radial distribution of γH2AX foci and the related modelling analysis. In few words, 3D coordinates are obtained for each γH2AX focus belonging to the same tissue slice with microscopy analysis. Based on visual inspection, foci are either assigned to the particle core or to the penumbra; the first are then used to reconstruct with a 3D fit the particle trajectory and thus the distance of each focus from the track centre. Similarly, 3D coordinates are also assigned to the centre of each cell nucleus. Starting from this information, a routine was implemented to reconstruct the volume associated to each nucleus in terms of voxels ($0.8 \times 0.8 \times 0.645\,\mu$m^3, average volume of cell nuclei corresponding to $65\,\mu$m^3). The voxelization procedure, as well as the use of a logarithmic binning for the analysis of the radial distance, allows to increase the resolution, especially at very short distances from the track centre. Experimental and modelling results are shown in fig. 2. Frequencies of measured foci per voxel are reported as a function of the distance from the track centre in a double-log scale. Results obtained with different experiments are pooled together. Remarkably, by extending the microscopy analysis to the whole tissue slice instead of restricting to the single cell, we were able to investigate for the first time the track structure over two-orders-of-magnitude distance in biological samples. When looking at the experimental data, we can identify three regions of interest: an inner saturation below about $0.5\,\mu$m (due to finite foci size, short-scale foci movement and sample processing), a decay region roughly proportional to the expected $1/r^2$ (shown for reference) and a plateau at large
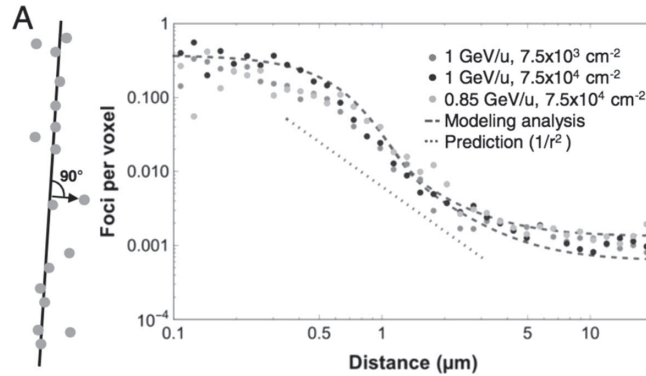
Fig. 2. – Radial distance analysis of γH2AX foci perpendicular to the trajectory. The lower and upper dashed curves represent the results of simulations based on LEM for fluences of 7.5×10^3 and 7.5×10^4 ions/cm^2, respectively. The dotted curve representing the theoretical $1/r^2$ dependency is shown for reference. Adapted with permission from Mirsch *et al.* [6].

distances, which can be associated to the overlap of the outer penumbra of multiple ion tracks that are not visible in the tissue slice. The saturation observed at short distances is also partially due to clustering of close-by DSB into the same γH2AX foci (*i.e.* cDSB in the LEM approach). The modelling analysis was performed by simulating with the LEM the track structure associated to 0.85 GeV/u Ti ions at the two fluences of interest. A Gaussian convolution was applied to the simulated dose profile in order to take into account for the deviations from the $1/r^2$ observed at short distances, while the plateau at large distances is considered as a background photon-like dose resulting from the contribution of the outer portion of many tracks (see original paper for details [6]). Finally, the information in terms of dose release was converted into foci induction, based on previous calibration experiments (suggesting an induction yield of 11.8 foci/cell/Gy) and taking also into account voxel dimension. A very good agreement is obtained between measured data and LEM simulations, which is supportive in general for the amorphous track structure approach adopted here. The comparison was made possible thanks to the biological measurement of track structure performed for the first time on such a large scale. These data will thus be very interesting to benchmark additional track structure codes.

4. – DNA DSB induction and rejoining

DNA DSB are attributed the greatest relevance in the induction of cell killing [26-28]. However, cells are able to process and eventually repair most part of the DSB produced by ionizing radiation. Several hypotheses have been proposed over the years trying to identify those sub-classes of DSB responsible for cell death. In the context of the LEM, a different severity is attributed to DSB according to their micrometre-scale clustering in chromatin loops. Results obtained by comparing modelling analysis to experimental data of DSB induction and rejoining will now be presented.

4`1. *DSB kinetic rejoining model*. – Based on the distinction of DSB into iDSB and cDSB, a kinetic rejoining model has been recently presented and applied to the analysis of a wide spectrum of experimental data previously obtained mainly by means of gel
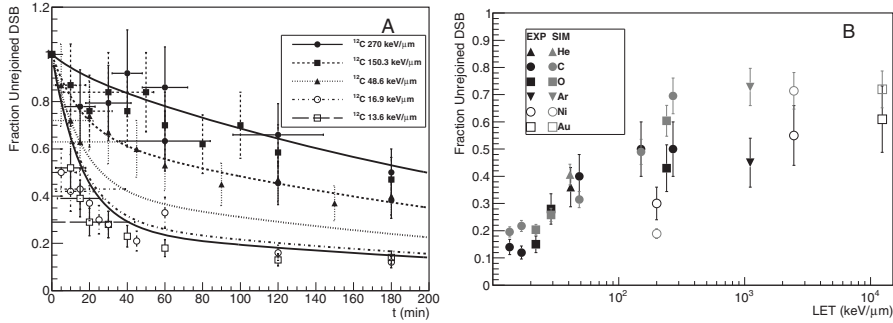
Fig. 3. – A: Experimental data (symbols) and predictions (lines) of DSB rejoining over time after irradiation of CHO-K1 cells with carbon ions at different energies ($\tau_{\text{fast}} = 9 \pm 1\,\text{min}$, $\tau_{\text{slow}} = 220 \pm 16\,\text{min}$); B: Remaining fractions of DSB 3 h after ion irradiation of CHO-K1 cells, experimental data (black) and model predictions (grey), half-lives are obtained by fitting an independent data set ($\tau_{\text{fast}} = 11 \pm 2\,\text{min}$, $\tau_{\text{slow}} = 428 \pm 126\,\text{min}$). For details about irradiation doses see the original manuscript. Adapted with permission from Tommasino *et al.* [7].

electrophoresis and filter elution techniques [7,9]. When DSB rejoining is measured over time after photon irradiation, typically a biphasic behavior is observed, with the majority of DSB rejoined in about half an hour after exposure, and a minor fraction persisting much longer. Generally, a slower rejoining is observed after ion irradiation compared to photons. It is thus intuitive trying to associate these fast and slow components of repair to DSB that are easy and complex to be processed, respectively. In the LEM framework, we proposed a link of the fast and slow repair to the iDSB and cDSB classes, respectively. Specifically, we developed a model where the LEM is used to calculate the expected statistics of iDSB and cDSB resulting from exposure to a specific ion radiation (particle type, energy/LET, dose), while Poisson statistics is adopted to describe photon irradiation. Then, the initial numbers of iDSB and cDSB are combined with a biphasic exponential decay function, having the fast and slow decay components associated to the processing of iDSB and cDSB, respectively. While the LEM (or Poisson statistics for photons) is used to provide input values in terms of DNA damage, the two half-lives for the fast and slow components are free fit parameters (see Tommasino *et al.* for details [7]).

This model has been tested against experimental data obtained with different cell lines, produced by different labs and including a large number of charged particles and energy/LET combinations [7,9]. Overall, promising results were obtained, supporting the relevance of the micrometre-scale DSB clustering for the explanation of the delayed DSB processing observed at high LET. A snapshot of these results is shown in fig. 3(A) where the model is used to fit DSB rejoining data obtained after irradiation of CHO-K1 cells with carbon ions at different energies. The LEM is used to calculate initial frequencies of iDSB and cDSB for a given LET, then a simultaneous fit is performed having the two half-lives as global fit parameters. The fraction of DSB processed by the fast component is obviously prominent at the lowest LET, while it gradually decreases for increasing LET. On the contrary, at the lowest energies (and highest LET), we only observe a single component of DSB rejoining, corresponding to the slow rejoining of cDSB representing now the large majority of induced damage. The model nicely fits extreme LET values, while some deviations are observed for the intermediate values. Importantly, the model has been also shown to be able to describe the dose-dependence observed in the kinetics of DSB rejoining after increasing doses of photon radiation [9].

In fig. 3(B) the predictive power of the model was also tested looking at the fraction of unrejoined DSB still present 3 h after irradiation as a function of particle species and LET. In this case, DSB induction patterns are obtained from the LEM in a LET range between 13.6 and 12350 keV/μm involving different particle species and combined with half-lives obtained by an independent fit in order to reproduce the experimental data. The model is now able to reproduce the trend observed in the experiments, with a tendency to overestimate the remaining fraction of DSB at the highest LET values. Remarkably, both measurements and predictions show a gradual increase in the remaining fraction of DSB for increasing LET, with a transition to a saturation-like behavior at high LET when the fraction of induced cDSB gets dominant.

Overall, this analysis supports not only the relevance of DSB clustering at the micrometre scale, but also the important role of higher-order chromatin structures as the Mbp-level loops for the explanation of the delayed rejoining observed for increasing LET, and more in general for DSB repair processes [7, 9].

4'2. *H2AX phosphorylation induction and processing*. – Based on the LEM approach, an extensive study has been recently published, where a combined experimental and modelling analysis is presented, aimed at the study of DSB induction and processing after photon irradiation, based on γH2AX flow cytometry measurements [29].

Compared to what discussed in the previous section, the analysis is complicated here by the fact that the observed foci are not point-like events, but rather involve an extended chromatin region. Furthermore, the kinetics of the γH2AX fluorescent signal and of DSB induction and repair are somewhat different [30]. In fact, while DSB starts to be rejoined directly after induction, the γH2AX signal reaches a maximum about 30–60 min after irradiation before slowly decaying when DSB are repaired. In order to take into account these aspects, the modelling strategy has been slightly modified (details elsewhere [29]). In few words, an additional kinetic component has to be considered for kinetics study, taking into account the initial rising of the fluorescence signal. While keeping distinguished the two half-lives for the processing of iDSB and cDSB, we consider the same kinetics describing the initial rising of the signal, independent of DSB complexity. Furthermore, it is assumed that iDSB and cDSB contribute equally in terms of fluorescence. This means that the full phosphorylation of hit loop/domains is expected, independent of the actual number of induced DSB. However, the fractions of iDSB and cDSB obviously still play a role concerning the complexity of the induced damage pattern, and thus on the DSB kinetics of rejoining. Additionally, the impact on the analysis of the possible 3D expansion of the phosphorylated region to an extended chromatin region has been also investigated, according to hypotheses recently appeared in the literature [31, 32]. This might lead to the spread of H2AX phosphorylation to loops surrounding the hit one, and is expected to have an effect on the measured fluorescent intensity but not on signal kinetics, being still dominated by iDSB and cDSB fractions.

Here we focus on the results obtained with the study of dose dependence of DSB rejoining after photon irradiation. Human skin fibroblasts were irradiated with increasing X-ray doses in the range 2–500 Gy and fixed at different time points from 1 to 24 h after exposure. The use of very high doses is motivated by the need to induce a significant component of cDSB with photon irradiation. γH2AX staining was performed and the fluorescent signal was measured with flow cytometry. Experimental data are shown in fig. 4(A), together with the fit analysis based on the LEM approach and described above. Assuming Poisson statistics for calculation of initial hit domains (combined with the 3D H2AX phosphorylation) and having the three half-lives as common fit parameters, good
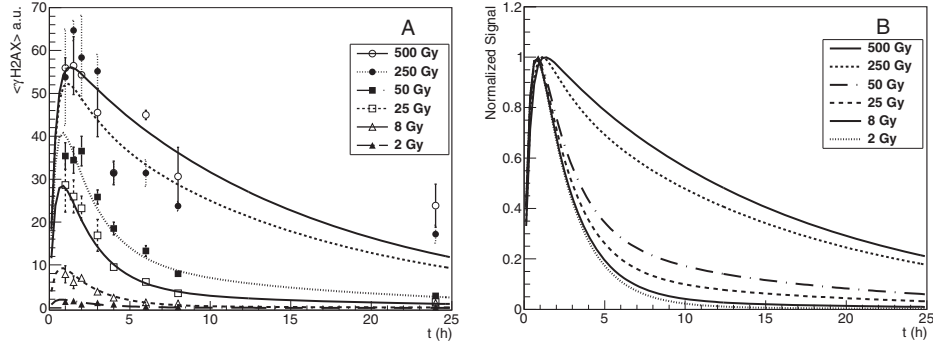
Fig. 4. – A: experimental data of flow cytometry measurements after irradiation with different X-rays doses (symbols) and corresponding application of the H2AX kinetic model (lines); error bars show standard error of the mean for at least two independent samples. Lines show the result of the fit ($\tau_{\text{fast}} = 1.48 \pm 0.10$ h, $\tau_{\text{slow}} = 10.50 \pm 0.59$ h), where the possibility of 3D extension of the H2AX phosphorylation was also considered [29]. B: comparison of model predictions for the different doses investigated after normalization to their maximum value of the functions plotted in panel A. Adapted from Tommasino et $al.$ [29]).

results are obtained. The fit curves were then normalized by their maximum values and plotted together in fig. 4(B). The comparison clearly shows a dose dependence in the kinetics of γH2AX signal disappearing. Specifically, in this approach the slowed-down repair for increasing doses is entirely due to a gradually increased fraction of induced cDSB. These results are in agreement with what previously published with the DSB kinetic rejoining model [9], and strongly support the relevance of micrometre-scale clustering of DSB as a key parameter for the description of the effects of radiation-induced DNA damage.

5. – Conclusions

Recent applications of the LEM to the study of basic radiobiological aspects have been partially reviewed here. Taken together, these results contribute to validate the picture of chromatin organization and of DNA damage induction on which the LEM is currently built. In fact, results obtained by combining modelling analysis with different experimental techniques support the relevance of the two DSB classes adopted in the LEM (iDSB and cDSB) for the interpretation of radiation effects induced at both low and high LET. Specifically, micrometre-scale DSB clustering into Mbp-level chromatin loops is found as a key aspect for the description of DSB repair processes. Obviously, in this simplified approach other aspects are neglected ($e.g.$ the role of eu- and hetero-chromatin, DSB clustering at the nanometre scale), which nevertheless are not in contradiction with what shown here but could rather complement and improve the agreement between model predictions and experimental data. Work is currently ongoing in the LEM group, aimed at testing further developments of the model, as for instance the consideration of different DSB sub-classes based on the complexity of the lesion at the nanometre scale, and on the implementation of cell cycle effects. The latter possibility has been already tested for the analysis of cell survival after photon irradiation, obtaining promising results [10]. Next step would now be to extend the cell cycle analysis to ion irradiation. Additional developments might include the replacement of the current fix domain size with a domain

size distribution for the description of chromatin organization. Prelminary evaluations in this direction have been already performed, but conclusions are hindered by the lack of experimental data describing loop structures at the micrometre scale. Finally, the remarkable outcomes of the track structure analysis not only support the amorphous track structure approach, but allowed revealing characteristics of energy depositions of charged particles in biological tissues with unprecedented resolution.

Apart from supporting the LEM approach for the description of radiation effects, the results summarized in this review suggest that significant advances can be obtained in radiation biology combining modelling analysis with experimental studies. This is especially true according to the increasing complexity of experimental techniques, often reflecting in the non-trivial interpretation of the measured data. The synergistic combination of advanced modelling tools with modern experimental methods could thus contribute shedding light on several open issues in the field of radiation biology.

$$* * *$$

REFERENCES

[1] JERMANN M., *Int. J. Part. Ther.*, **2** (2015) 50.
[2] DURANTE M. and LOEFFLER J. S., *Nat. Rev. Clin. Oncol.*, **7** (2010) 37.
[3] TOBIAS C. A. *et al.*, *Int. J. Radiat. Oncol. Biol. Phys.*, **8** (1982) 109.
[4] SCHOLZ M. *et al.*, *Radiat. Environ. Biophys.*, **36** (1997) 59.
[5] ELSÄSSER T. *et al.*, *Int. J. Radiat. Oncol. Biol. Phys.*, **78** (2010) 1177.
[6] MIRSCH J. *et al.*, *Proc. Natl. Acad. Sci. USA*, **112** (2015) 12396.
[7] TOMMASINO F. *et al.*, *Radiat. Res.*, **180** (2013) 524.
[8] HERR L. *et al.*, *PLOS ONE*, **9** (2014) e83923.
[9] TOMMASINO F. *et al.*, *Radiat. Prot. Dosim.*, **166** (2015) 66.
[10] HUFNAGL A. *et al.*, *DNA Repair*, **27** (2015) 28.
[11] ELSÄSSER T. *et al.*, *Radiat. Res.*, **167** (2007) 319.
[12] KIEFER J. *et al.*, *Phys. Med. Biol.*, **31** (1986) 1201.
[13] ELSÄSSER T. *et al.*, *Int. J. Radiat. Oncol. Biol. Phys.*, **71** (2008) 866.
[14] YOKOTA H. *et al.*, *J. Cell Biol.*, **130** (1995) 1239.
[15] SOLOVJEVA L. *et al.*, *Chromosome. Res.*, **6** (1998) 595.
[16] FRIEDRICH T. *et al.*, *Radiat. Prot. Dosim.*, **166** (2015) 61.
[17] FRIEDRICH T. *et al.*, *Radiat. Res.*, **178** (2012) 385.
[18] FRIEDRICH T. *et al.*, *Int. J. Radiat. Biol.*, **88** (2012) 103.
[19] NEUMAIER T. *et al.*, *Proc. Natl. Acad. Sci. USA*, **10** (2012) 443.
[20] FRIEDRICH T. *et al.*, *Acta. Oncol.*, **52** (2013) 589.
[21] EMFIETZOGLOU D. *et al.*, *Nucl. Instrum. Methods Phys. Res. B*, **209** (2003) 239.
[22] DINGFELDER M. *et al.*, *Radiat. Res.*, **169** (2008) 584.
[23] ROGAKOU E. P. *et al.*, *J. Biol. Chem.*, **273** (1998) 5858.
[24] ROTHKAMM K. and HORN S., *Ann. Ist. Super. Sanità*, **45** (2009) 265.
[25] MACPHAIL S. H. *et al.*, *Int. J. Radiat. Biol.*, **79** (2003) 351.
[26] BANATH J. P. *et al.*, *Cancer Res.*, **64** (2004) 7144.
[27] WADA S. *et al.*, *J. Vet. Med. Sci.*, **67** (2005) 1089.
[28] MIRZAYANS R. *et al.*, *Int. J. Radiat. Oncol. Biol. Phys.*, **66** (2006) 1498.
[29] TOMMASINO F. *et al.*, *PLOS ONE*, **10** (2015) e0129416.
[30] KINNER A. *et al.*, *Nucleic. Acids. Res.*, **36** (2008) 5678.
[31] MUÑOZ D. P. *et al.*, *Nucleic. Acids. Res.*, **41** (2013) 2894.
[32] SAVIC V., *Front. Genet.*, **4** (2013) 139.